Title: Infrared chemical imaging: spatial resolution evaluation and super-resolution concept

Authors: Marc Offroy, Yves Roggo, Peyman Milanfar, Ludovic Duponchel

PII: S0003-2670(10)00791-9
DOI: doi:10.1016/j.aca.2010.06.025
Reference: ACA 230638

To appear in: *Analytica Chimica Acta*

Received date: 4-3-2010
Revised date: 17-6-2010
Accepted date: 21-6-2010

Please cite this article as: M. Offroy, Y. Roggo, P. Milanfar, L. Duponchel, Infrared chemical imaging: spatial resolution evaluation and super-resolution concept, *Analytica Chimica Acta* (2010), doi:10.1016/j.aca.2010.06.025

Infrared chemical imaging: spatial resolution evaluation and super-resolution concept

Marc Offroy, [a] *Yves Roggo,* [b] *Peyman Milanfar,* [c] *Ludovic Duponchel* [*,a]

(a) Laboratoire de Spectrochimie Infrarouge et Raman, LASIR, CNRS UMR 8516, Bât. C5, Université des Sciences et Technologies de Lille, 59655 Villeneuve d'Ascq Cedex, France.

(b) F. Hoffmann-La Roche A.G., Basel, Switzerland.

(c) Multi-Dimensional Signal Processing Laboratory, Electrical Engineering Department, Baskin School of Engineering, University of California, 1156 High Street, Mailcode SOE2, Santa Cruz, CA 95064, U.S.A.

* Corresponding author. Phone: +33 320436661. Fax: +33 320436755. Email : ludovic.duponchel@univ-lille1.fr

ABSTRACT

Chemical imaging systems help to solve many challenges in various scientific fields. Able to deliver rapid spatial and chemical information, modern infrared spectrometers using Focal Plane Array detectors (FPA) are of great interest. Considering conventional infrared spectrometers with a single element detector, we can consider that the diffraction-limited spatial resolution is more or less equal to the wavelength of the light (i.e. 2.5 to 25 μm). Unfortunately, the spatial resolution of FPA spectroscopic setup is even lower due to the detector pixel size. This becomes a real constraint when micron-sized samples are analysed. New Chemometrics methods are thus of great interest to overcome such resolution drawback, while keeping our far-field infrared imaging spectrometers. The aim of the presented work is to evaluate the super-resolution concept in order to increase the spatial resolution of infrared imaging spectrometers using FPA detectors. The main idea of super-resolution is the fusion of several low-resolution images of the same sample to obtain a higher-resolution image. Applying the super-resolution concept on a relatively low number of FPA acquisitions, it was possible to observe a 30 % decrease in spatial resolution.

KEYWORDS: Super-resolution, Chemometrics, Infrared Imaging, Focal Plane Array Detector, Spatial Resolution.

INTRODUCTION

Fourier Transformed Infrared Spectroscopic imaging is a valuable tool in order to obtain information concerning the molecular distribution of various compounds in complex samples. FTIR spectrometers are thus coupled with microscopes to enable the spectral analysis of physically small samples or even to focus on specific regions of these. The spatial resolution of a microscope is ideally determined by diffraction of the selected radiation. When a point source monochromatic radiation is passed through the microscope, the well known Airy pattern is observed at the beam focus. The central circular area, the Airy disc has thus a radius r given by:

$$r = 0.61.(\lambda / NA) \quad (1)$$

with λ the wavelength of the radiation and NA the numerical aperture of the microscope. Considering the previous equation, two objects are completely resolved if they are separated by $2r$ and hardly resolved with r (Rayleigh criterion of resolution). In this way, one can consider that the diffraction-limited spatial resolution is more or less equal to the wavelength of the light when conventional Cassegrainian objectives are used in the air. Unfortunately, this relation is never observed for many reasons. First, the detector is not a point and has a finite size. The pixel detector becomes a sort of aperture. When the pixel size of the sample plane is higher than the wavelength, the system is said to be 'pixel size-limited' [1]. In these conditions, the spatial resolution is limited by pixel size and less by diffraction phenomenon. Second, a low axial spatial resolution (z-direction, depth of the sample) can degrade the achievable optimal lateral spatial resolution. Third, optical setup of the microscope has a direct influence on the spatial resolution. The number of aperture in the optical pathway is an example [2,3]. For all the above reasons, it is often impossible to find and use a theoretical model in order to evaluate the spatial resolution of a micro-spectrometer particularly when Focal Plane Array detectors are used. The preferred approach is to propose a direct estimation based on real measurements for the considered instrumental setup.

Even if the evaluation of spatial resolution is not straightforward, the main issue comes from its intrinsic value observed in mid infrared spectral range (2.5-25 μm). Considering few microns-sized samples, the spatial resolution of far-field infrared imaging spectrometers is always too low in order to observe many details. The aim of the presented work is thus to propose the super-resolution concept in order to increase the spatial resolution of infrared imaging spectrometers using FPA detectors. Super-resolution is defined by the use of image processing algorithms in order to overcome the limitations of optical systems [4,5,6]. The main idea of super-resolution is the fusion of several low-resolution images (LR) of the same object to obtain a high-resolution image (HR) [7,8,9]. The first paper dealing with recovering high resolution image using multi-frames was written by Tsai and Huang [10]. It was shown that fusing under-sampled low resolution images with relative sub-pixel motion could give a super-resolution image with few or no aliasing effects. The first paper dealing with super-resolution and vibrational spectroscopy was published recently by Duponchel and co-workers [11]. Very interesting results were presented in the field of Raman imaging. The main novelty of this paper is applying super-resolution concept to FTIR imaging.

EXPERIMENTAL

Spatial resolution evaluation methods

There are numerous experimental methods to estimate the spatial resolution of an imaging system [12,13]. The purpose of the presented work is not to find the best one but to propose a precise technique to objectively and quantitatively estimate the improvement brought by the new concept of super-resolution.

The first method is called ‘step-edge’ or the ‘knife-edge’ [14]. The main idea is to observe a step on the considered sample. Considering the knife-edge as the input to an optical system, then the signal along the perpendicular direction to the edge is the Line Spread Function (LSF) (Figure 1a). The derivative of the LSF with respect to position is the Point Spread Function (PSF) in the considered direction. The PSF is the response of the system to a point source observation. The latter function is then

used as a measure of resolution by calculating its full width at half maximum (FWHM). The second method uses the Rayleigh's criterion in order to determine whether a pattern of identical consecutive bars are resolved or not (Figure 1b). Considering now the signal along the perpendicular axis to the bars, if the signal between two consecutive peaks (S) is less than $8/\pi^2$ (i.e. 81 %) of the intensity of the peak (S_{max}), then the two bars are declared resolved. The resolution is meant here as the distance between the two signal maxima considering the smallest resolved bars.

Materials

In order to evaluate the spatial resolution and explore the super-resolution concept, all spectroscopic measurements were done on the 1951 USAF resolution target. This chart is a resolution test pattern conformed to the MIL-STD-150A standard, set by US Air Force in 1951. The resolution target a has chrome metal coating pattern on soda-lime glass. It is an appropriated sample for the infrared imaging experiment: contrasted images are obtained due to the high reflectivity of metal and the high absorbance of glass. The pattern consists of groups of three bars with dimensions going from large to small. More precisely, it consists of nine "groups" divided in five layers of patterns (Figure 2). The largest groups, forming the first layer, are located on the outer sides. The smaller layers repeat the same pattern but are progressively smaller toward the center. Each group consists of six elements, numbered from 1 to 6 (except for group 9). Within the same layer, the odd-numbered groups appear contiguously from 1 through 6 from the upper right corner. The first element of the even-numbered groups is at the lower right of the layer, with the remaining 2 through 6, at the left. As described in Figure 2, the scales and dimensions of the bars depend of the spatial frequency LP i.e. the number of line pairs per mm. Given the group *g* and the element *e*, the spatial frequency is determined by the Equation:

$$\mathrm{LP} = 2^{\left[g + \left(\frac{e-1}{6}\right)\right]} \text{ (unit: line pairs / mm)} \quad (2)$$

Table 1 shows the evolution of the spatial frequency and the line width (LW) for a given element. As it can be noticed, it is even possible (if necessary) to analyse patterns with sub-wavelength dimensions from high group numbers considering the mid infrared spectral range (2.5 to 25 μm).

FT-IR measurements

An Equinox 55 spectrometer (Bruker, Ettlingen, Germany) coupled with a Hyperion 3000 microscope equipped with a 64 × 64 Mercury-Cadmium-Telluride Focal Plane Array (MCT-FPA) detector was used to acquire the IR reflectance spectra between 3900 and 900 cm^{-1} at 32 cm^{-1} resolution under N_2 purge. After signal integration at a defined wavenumber from reflectance spectra, it was thus possible to obtain an image of 64 × 64 pixels. The number of scans was 5 corresponding to an acquisition time of few seconds. The surface analyzed by one FPA measurement was a 270 μm × 270 μm area due to the x15 Cassegrainian objective (*NA*=0.45). The pixel size of the sample plane was thus 4.22 μm x 4.22 μm on raw FPA measurements. Between two FPA measurements, it was possible to move the sample with a XY-motorized stage with a repeatability of 0.1 μm in position.

Super-resolution concept

The aim of this part is to describe a global framework of the super-resolution concept. More detailed procedures can be found in numerous papers [4,5,9]. As in image processing papers, images are represented column-wise lexicographically ordered for matrix notation convenience. Given are N measured low resolution images $\{\underline{Y}_k\}_{k=1}^{N}$, where each image is defined by $M \times M$ pixels and represented by the unfolded matrice $\underline{Y}_k$ of size $[M^2 \times 1]$. These LR images are different representations of a single HR image (L x L pixels) represented by the unfolded matrice $\underline{X}$ of size $[L^2 \times 1]$, where L > M for $1 \le k \le N$. Considering 16 FPA measurements for our experiment, N = 16, M = 64 and L = 256. L is a user defined parameter satisfying the rule of thumb:

$$L^2 < NM^2 \quad (3)$$

In fact, it can be considered that each LR image measured is the result of a particular geometric warping (translations in our microspectrometric case), linear space-invariant blurring and uniform rational decimation performed on the ideal HR image $\underline{X}$. Additive Gaussian noise is also considered corrupting the low resolution images. It is thus possible to propose an analytical model (eq. 4), in order to express the steps described previously:

$$\underline{Y}_k = D_k H_k F_k \underline{X} + \underline{V}_k \quad (4)$$

The matrix F_k of size $[L^2 \times L^2]$ corresponds to the geometric warp operation between the $\underline{X}$ image and $\underline{Y}_k$. The matrix H_k of size $[L^2 \times L^2]$ is the blur matrix defined by the optical system's Point Spread Function. The matrix D_k of size $[M^2 \times L^2]$ corresponds to the decimation resulting in $\underline{Y}_k$. In other words, this step corresponds to the reduction of the number of observed pixels in the measured images. The additive Gaussian noise observed in the *k*-th measurement is described by the vectors $\{\underline{V}_k\}_{k=1}^{N}$ with zero mean. In this way, super-resolution is an inverse problem since $\underline{X}$ has to be found from known low resolution images $\{\underline{Y}_k\}_{k=1}^{N}$. It is necessary to evaluate D_k, H_k and F_k matrices for all $k = 1...N$ in order to resolve (eq. 4), For our spectroscopic experiment F_k are just defined by the motion between low resolution images $\{\underline{Y}_k\}_{k=1}^{N}$ and one of the low resolution images (such as, say, $\underline{Y}_1$) chosen as a reference. These motions are micron (sub-pixelic) translations induced by the XY stage between two FPA measurements. Concerning H_k blur matrices, we consider that all low resolution images are obtained with the same optical system and thus viewed through the same PSF that is to say $\forall k, H_k = H$. H is usually estimated from a spatial resolution evaluation but even a rough guess of it like a Gaussian filter can be used. The matrix D_k depends only on the decimation ratio between the HR image and the measured LR image i.e. the ratio between the number of pixel in the LR image M^2 and the HR image L^2. Considering a generalization of the analytical model (eq. 4) applied on all *N* given LR images we have:

$$\begin{bmatrix} \underline{Y}_1 \\ \vdots \\ \underline{Y}_N \end{bmatrix} = \begin{bmatrix} \underline{D}_1\underline{H}_1\underline{F}_1 \\ \vdots \\ \underline{D}_N\underline{H}_N\underline{F}_N \end{bmatrix} \underline{X} + \begin{bmatrix} \underline{V}_1 \\ \vdots \\ \underline{V}_N \end{bmatrix} \quad (5)$$

It is now possible to retrieve the HR image $\underline{X}$ with many classical restoration methods like *Maximum A Posteriori* estimation [15,16,17,18,19]. Due to the high dimension of the equation system (Eq. 5) and inherent numerical instability of such inverse problems, regularization procedure are also necessary in order to find a stable solution of $\underline{X}$. Several regularizations methods like Bilateral Total Variation and Tikhonov were tested but we only present in this paper the best resolution results obtained with the "Norm 1 + Bilateral Total Variation" algorithm [4,5]. Matlab v 7.1 computing environment (The Mathworks, MA, USA) and the multi-dimensional signal processing (MDSP) toolbox [20] were used for all calculations reported below. More details about the whole procedure can be found in our previous work dealing with Raman imaging [11]. From a practical point of view, the super-resolution calculation is not time consuming since it takes only few minutes with a personal computer.

RESULTS AND DISCUSSION

Spatial resolution evaluation

The first objective of the presented work was to estimate the advantages and inconveniences of the 'step-edge' and the 'Rayleigh criterion' methods. Figure 3 illustrates the application of these two methods on an infrared test chart image at 3600 cm^{-1} for the evaluation of the spatial resolution along the *x* direction. Both A and B white arrows indicate zones where the 'step-edge' method was applied while the black ones indicate zones where the 'Rayleigh's criterion' was used (element 1 group 5 to element 5 group 6). On Rayleigh's criterion bars profiles, the green dotted lines represent the limit of $8/\pi^2$ for the S_{max}/S ratio. It can be observed without ambiguity that bars are resolved from the element 1 group 5 to element 3 group 6 because the S minima are always below this limit. Since the element 5 group 6 are not resolved, the effective resolution is thus between these elements and the element 5 group 6. Considering the characteristics of these elements (Table 1), the resolution would be between 9.84 µm

(2 x LW_{G6E5}) and 12.40 µm (2 x LW_{G6E3}). Thus this method is not so accurate and rather difficult to use. Firstly, there is a dependency with the size of consecutive patterns proposed on the test chart. Any intermediate value of resolution is impossible to estimate. Secondly, considering smaller patterns, the bars profiles are defined by an lower number of points . Thus it becomes really difficult to observe the real minima and maxima. In this way, the real S_{max}/S ratio cannot be estimated and the comparison with the $8/\pi^2$ is risky. It is even more difficult to appreciate the ratio because the C contrast always decreases for smaller patterns.

$$C = \frac{S_{max} - S_{min}}{S_{max} + S_{min}} \quad (6)$$

The last problem is the number of FPA measurements necessary for the analysis of all bars profiles. In our case, three FPA acquisitions are necessary in order to observe all profiles from element 1 group 5 to element 5 group 6 due to the fact that the analysed region of one FPA measurement is only 270 µm x 270 µm. The 'step-edge' method is less restrictive and more accurate. In our example (Figure 3), the derivative of the 'Step-edge A' profile obtained from only one line of a single FPA acquisition allows, after a Gaussian fit, to find a resolution of 9.19 µm. The same procedure applied on the step-edge B (square with smaller dimensions) gives a consistent result of 9.13 µm. It is obvious that the precision of this method is related to the number of experimental points on the LSF. When possible, a higher number of points should be used in order to obtain a better Gaussian fit and a more accurate resolution. So in this example, 'Step-edge A' profile is preferred. Moreover, a single FPA measurement gives several evaluations of the resolution by the analysis of successive and parallel LSF in the same zone. It is then possible to propose an error for the evaluation of the resolution. Therefore the quality of the proposed method is demonstrated.

Figures 4a and 4b present the evaluation of the spatial resolution from raw FPA images at different wavenumbers in the *x* and *y* directions. For each wavenumber, 17 different LSF profiles are used in order to evaluate dispersion of the resolution. We use a classical boxplot representation for which the bottom and top of the box are the 25th and 75th percentile, the bold band near the middle of

the box is the median, the ends of the whiskers are the lowest resolution still within 1.5 IQR (Interquartile range) of the lower quartile, and the highest resolution still within 1.5 IQR of the upper quartile, and circle are the outliers. The dotted line is the mean resolution value. It can be observed that for a given wavenumber the resolution dispersion is rather low indicating the robustness of the 'Step-edge' method. Moreover it was shown that resolution is wavelength dependent i.e. the higher wavenumber the better resolution. Nevertheless it does not follow Eq. (1) because the system is not diffraction limited but pixel size-limited. Comparing Figure 4a and 4b, one can notice that spatial resolution is not the same in x and y direction. This is due to the instrumental setup. In fact, a half mirror instead of a beam splitter is used to direct the IR light into the objective. With this device, the full numerical aperture of the objective is only used in the parallel direction to the half mirror (*x* direction). In the perpendicular direction to the half mirror (*y* direction), only the half numerical aperture is available. Therefore the spatial resolution is different for the two directions. In order to obtain the same resolution in *x* and *y* direction, it would be necessary to use a beam splitter in order to direct the IR light into the objective. Nevertheless, considering the reflexion mode, in this case only 25 % of the light would finally reach the detector compared to the 50 % obtained for our half mirror setup.

Super-resolution concept evaluation

The raw low resolution images were obtained successively by moving the sample with a micron step (sub-pixelic moves) in the *x* and *y* directions between FPA measurements. Figure 5 presents the application of the super-resolution concept on 16 raw FPA images at 3600 cm^{-1}. This global number of FPA images was optimized in order to obtain a better spatial resolution within a reasonable time for all spectroscopic analysis (less than 1 minute). First we notice visually the uncontested improvement of the spatial resolution between the original FPA and the super-resolved image. Moreover, the 'step-edge' method applied to this new image gives a resolution of 6.09 μm compared to 9.13 μm at the same wavenumber in Figure 3. Considering the super-resolution method as an over-sampling technique is a counterintuitive idea. There are indeed more points on the LSF but its shape is also narrower. Figure 6a

and 6b present the evaluation of the spatial resolution of super-resolved images at different wavenumbers in *x* and *y* direction. Comparing these results with Figure 4, one observes a 30% improvement for the spatial resolution in both directions and all wavenumbers which is a rather spectacular result. It can be also noticed that the dispersion on the evaluation of the resolution is less important for super-resolved images than for raw FPA images at a given wavenumber. This is mainly due to a higher image signal to noise ratio obtained with the super-resolution algorithm. Figure 7 proposes a visual representation of this improvement according to the wavenumber.

CONCLUSION

This work presents the first attempt to use super-resolution methodology applied to FTIR imaging spectroscopy. In the first part of the paper, it was proposed to evaluate the 'step-edge' and the 'Rayleigh Criterion' methods for the measurement of the spatial resolution. The 'step-edge' method was the more accurate and the easier to use. Applying the super-resolution concept on a relatively low number of FPA acquisitions, it was possible to observe a 30 % improvement in the spatial resolution. It is a very important result since FPA imaging spectrometers have in general a rather low spatial resolution. Future works will be focused on the study of factors affecting the performance of multi-frame super-resolution restoration. It will be interesting to apply super-resolution on another FPA spectrometer with a higher density pixel and a higher magnification objective for which the spatial resolution is more dictated by wavelength-limited diffraction than the pixels size. Another challenge will be to use super-resolution on time resolved FPA measurements in order to propose chemical images over time with a higher spatial resolution. Finally, super-resolution has to be tested on infrared spectrometers with single element detector in order to know if sub-wavelength imaging is possible.

FIGURE CAPTIONS

Figure 1. Spatial resolution evaluation with a) the 'Step-edge' method and b) the 'Rayleigh's criterion' method.

Figure 2. The 1951 USAF resolution target used for all spectroscopic measurements. (LP = line Pairs / mm)

Figure 3. Spatial resolution evaluation along the *x* direction on an infrared test chart image at 3600 cm^{-1}.

Figure 4. Spatial resolution evaluation of raw FPA images at different wavenumbers in a) *x* and b) *y* directions.

Figure 5. Application of the super-resolution concept on 16 raw FPA images at 3600 cm^{-1}. Spatial resolution of the super-resolved image.

Figure 6. Spatial resolution evaluation of super-resolved images at different wavenumbers in a) *x* and b) *y* directions.

Figure 7. Visualization of the spatial resolution improvement at various wavenumbers.

TABLE CAPTIONS

Table 1. Evolution of the spatial frequency LP (number of line pairs / mm) and the line width (LW) for a given element in a group for the USAF test chart.

284 **REFERENCES**

[1] R. Salzer, H.W. Siesler, Infrared and Raman spectroscopic imaging, Wiley-VCH (2009).

[2] A.J. Sommer, J.E. Katon, Appl. Spectrosc. 45 (1991) 1633.

[3] N. Teramae, T. Nishikoda, Infrared Microscopy, IPC Publisher, Tokyo (2003).

[4] S. Farsiu, M.D. Robinson, M. Elad, P. Milanfar, IEEE trans. image process, 13 (2004), 1327.

[5] S. Farsiu, D. Robinson, M. Elad, P. Milanfar, Int. j. imaging syst. technol., 14 (2004) 47.

[6] M.K. Ng, N.K. Bose, IEEE signal process. mag., 20 (2003) 62.

[7] S.C. Park, M.K Park, M.G. Kang, IEEE signal process. mag., 20 (2003) 21.

[8] M.M. Hadhoud, F. Abd El-Samie, S.E. El-Khamy, Proc. IEEE Conf. 4th Workshop Photon. and Appl., (2004) 2.

[9] N. Nguyen, P. Milanfar, G. Golub, IEEE trans. image process., 10 (2001) 573.

[10] R.Y. Tsai, T.S. Huang, Advances in Computer Vision and Image Processing, JAI Press, 1984.

[11] L. Duponchel, P. Milanfar, C. Ruckebusch, J-P. Huvenne, Anal. Chim. Acta, 607 (2008) 168.

[12] P. Lasch, D. Naumann, BBA-Biomembranes 1758 (2006) 814.

[13] E.H.K. Stelzer, J. Microscoc. 189 (1998) 15.

[14] E. Levenson, P. Lerch, M. Martin, Infrared Phys. Techn. 49 (2006) 45.

[15] M. Elad, Y. Hel-Or, IEEE trans. image process., 10 (2001) 1187.

[16] R.C. Hardie, K.J. Barnard, E.E. Armstrong, IEEE trans. image process., 6 (1997) 1621.

[17] R.R. Schultz, R.L. Stevenson, IEEE trans. image process., 3 (1994) 233.

[18] A.J. Patti, M.I. Sezan, A.M. Tekalp, IEEE trans. image process., 6 (1997) 1064.

[19] S. Chaudhuri, Super-Resolution Imaging. Springer Ed., 2001.

[20] http://users.soe.ucsc.edu/~milanfar/software/superresolution.html

Table 1

Group Number										
	0		1		2		3		4	
Element	LP / mm	LW (μm)	LP / mm	LW (μm)	LP / mm	LW (μm)	LP / mm	LW (μm)	LP / mm	LW (μm)
1	1.00	500.00	2.00	250.00	4.00	125.00	8.00	62.50	16.00	31.25
2	1.12	445.45	2.24	222.72	4.49	111.36	8.98	55.68	17.96	27.84
3	1.26	396.85	2.52	198.43	5.04	99.21	10.08	49.61	20.16	24.80
4	1.41	353.55	2.83	176.78	5.66	88.39	11.31	44.19	22.63	22.10
5	1.59	314.98	3.17	157.49	6.35	78.75	12.70	39.37	25.40	19.69
6	1.78	280.62	3.56	140.31	7.13	70.15	14.25	35.08	28.51	17.54

Group Number										
	5		6		7		8		9	
Element	LP / mm	LW (μm)	LP / mm	LW (μm)	LP / mm	LW (μm)	LP / mm	LW (μm)	LP / mm	LW (μm)
1	32.00	15.63	64.00	7.81	128.00	3.91	256.00	1.95	512.00	0.98
2	35.92	13.92	71.84	6.96	143.68	3.48	287.35	1.74	574.70	0.87
3	40.32	12.40	80.63	6.20	161.27	3.10	322.54	1.55	645.08	0.78
4	45.25	11.05	90.51	5.52	181.02	2.76	362.04	1.38	-	-
5	50.80	9.84	101.59	4.92	203.19	2.46	406.37	1.23	-	-
6	57.02	8.77	114.04	4.38	228.07	2.19	456.14	1.10	-	-

Figure 1

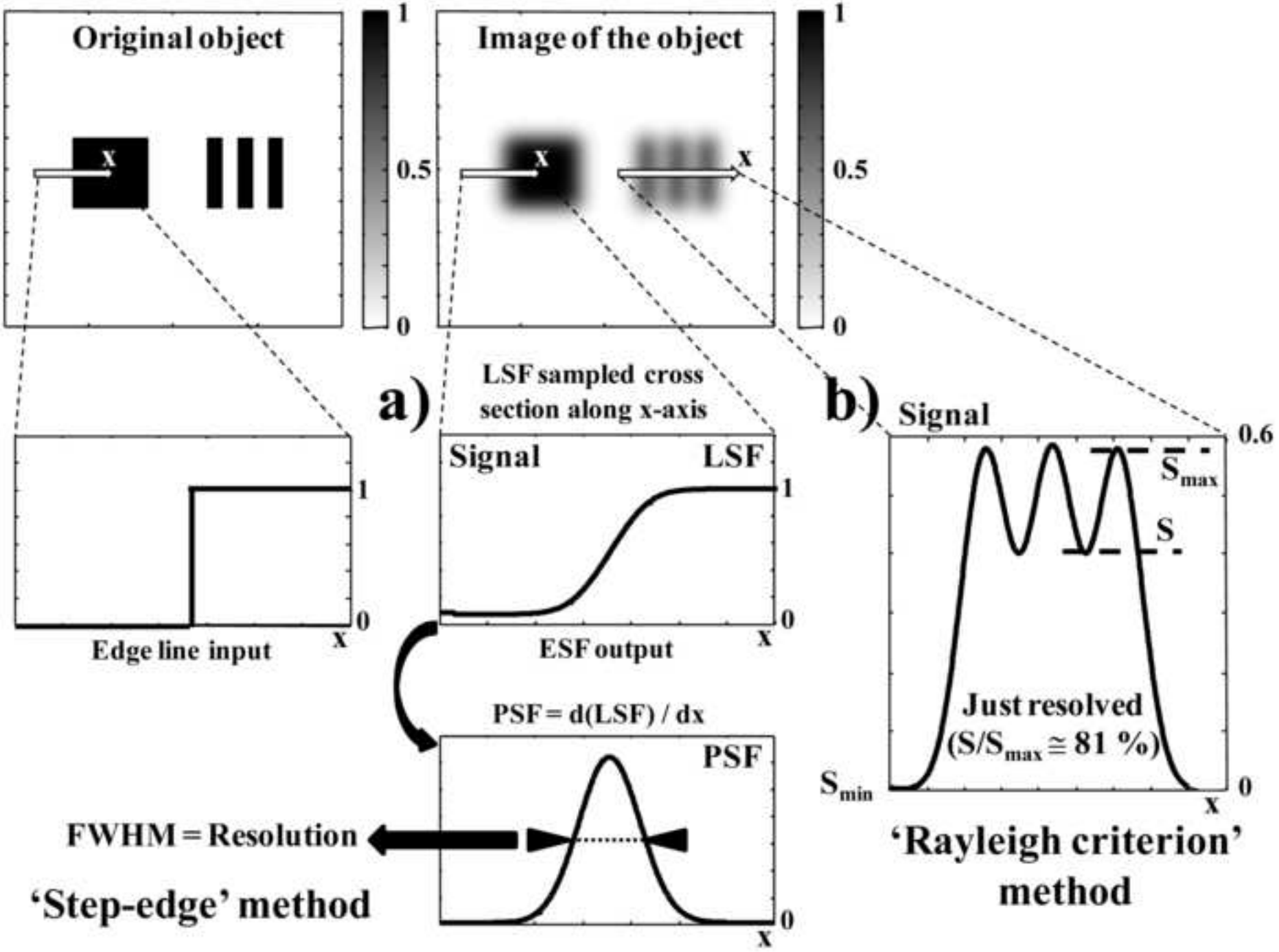
Original object
Image of the object
1
0.5
0
x
a)
LSF sampled cross section along x-axis
Signal
LSF
Edge line input
ESF output
PSF = d(LSF) / dx
PSF
FWHM = Resolution
'Step-edge' method
b)
Signal
0.6
S_{max}
S
S_{min}
Just resolved
($S/S_{max} \cong 81$ %)
'Rayleigh criterion' method

Figure 2

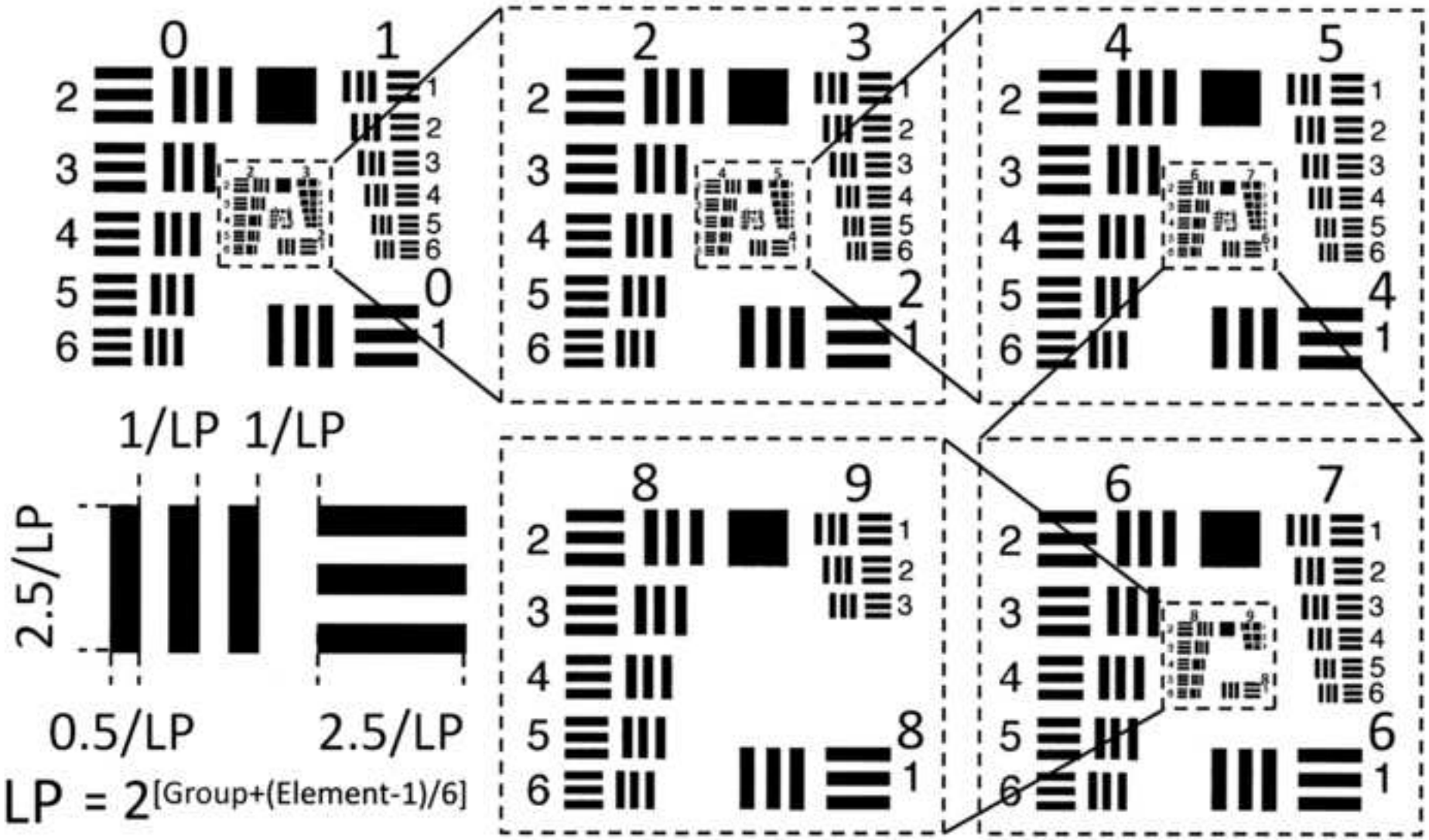

Figure 3

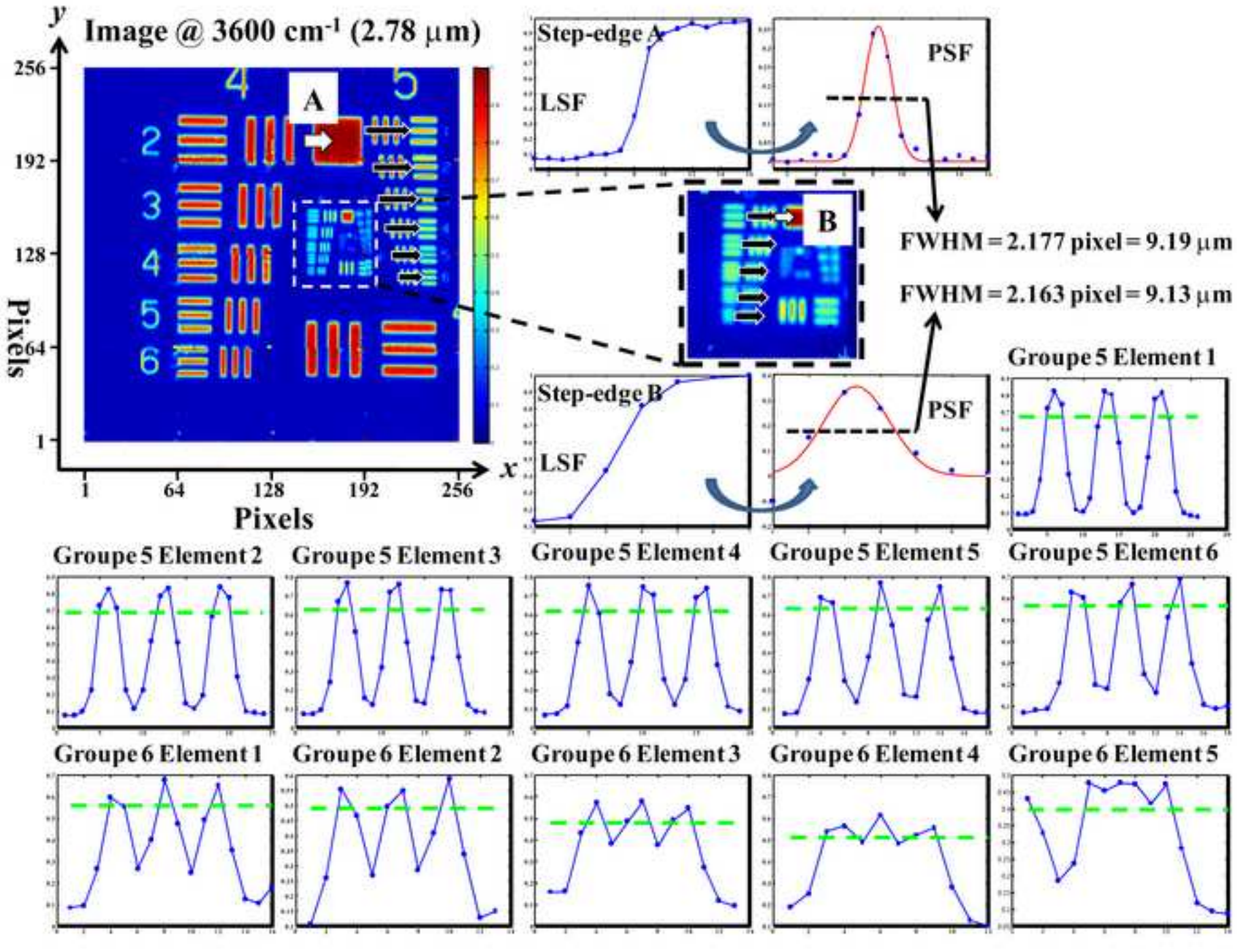
Image @ 3600 cm-1 (2.78 μm)
y
x
Pixels
256
192
128
64
1
A
B
2
3
4
5
6
Step-edge A
LSF
PSF
FWHM = 2.177 pixel = 9.19 μm
Step-edge B
LSF
PSF
FWHM = 2.163 pixel = 9.13 μm
Groupe 5 Element 1
Groupe 5 Element 2
Groupe 5 Element 3
Groupe 5 Element 4
Groupe 5 Element 5
Groupe 5 Element 6
Groupe 6 Element 1
Groupe 6 Element 2
Groupe 6 Element 3
Groupe 6 Element 4
Groupe 6 Element 5

Figure 4

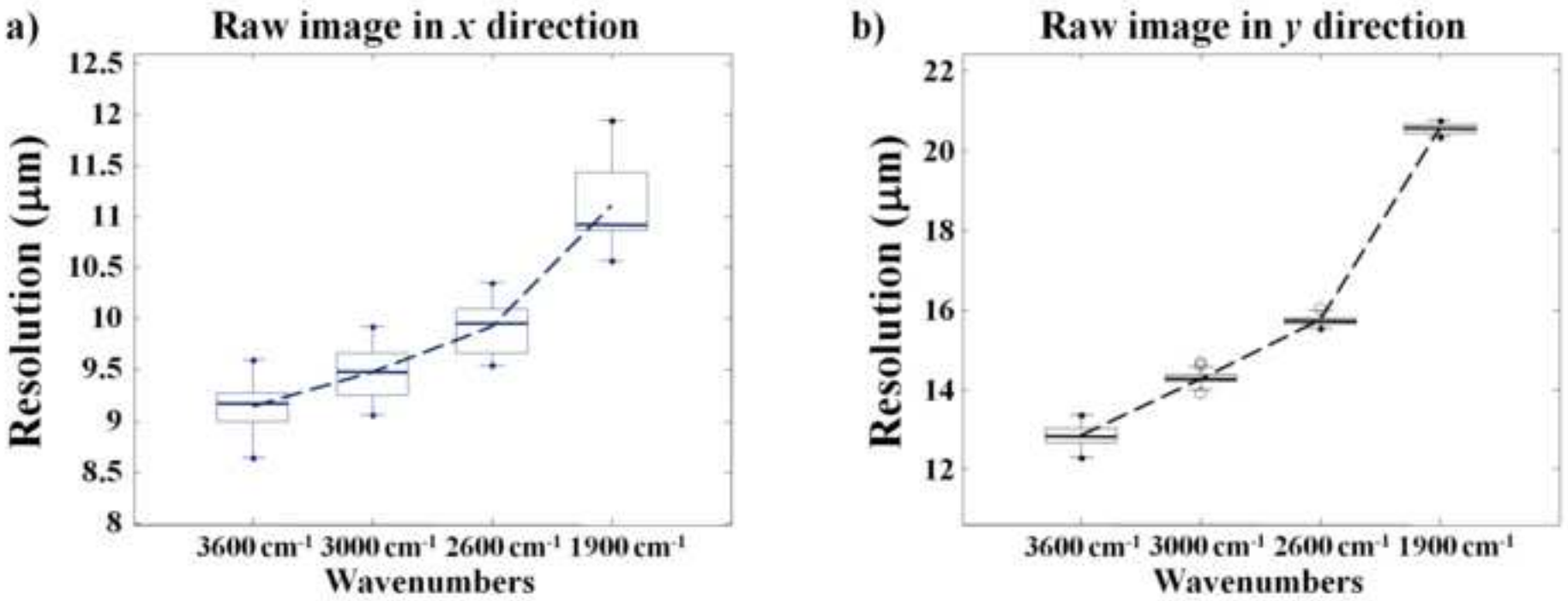

Figure 5

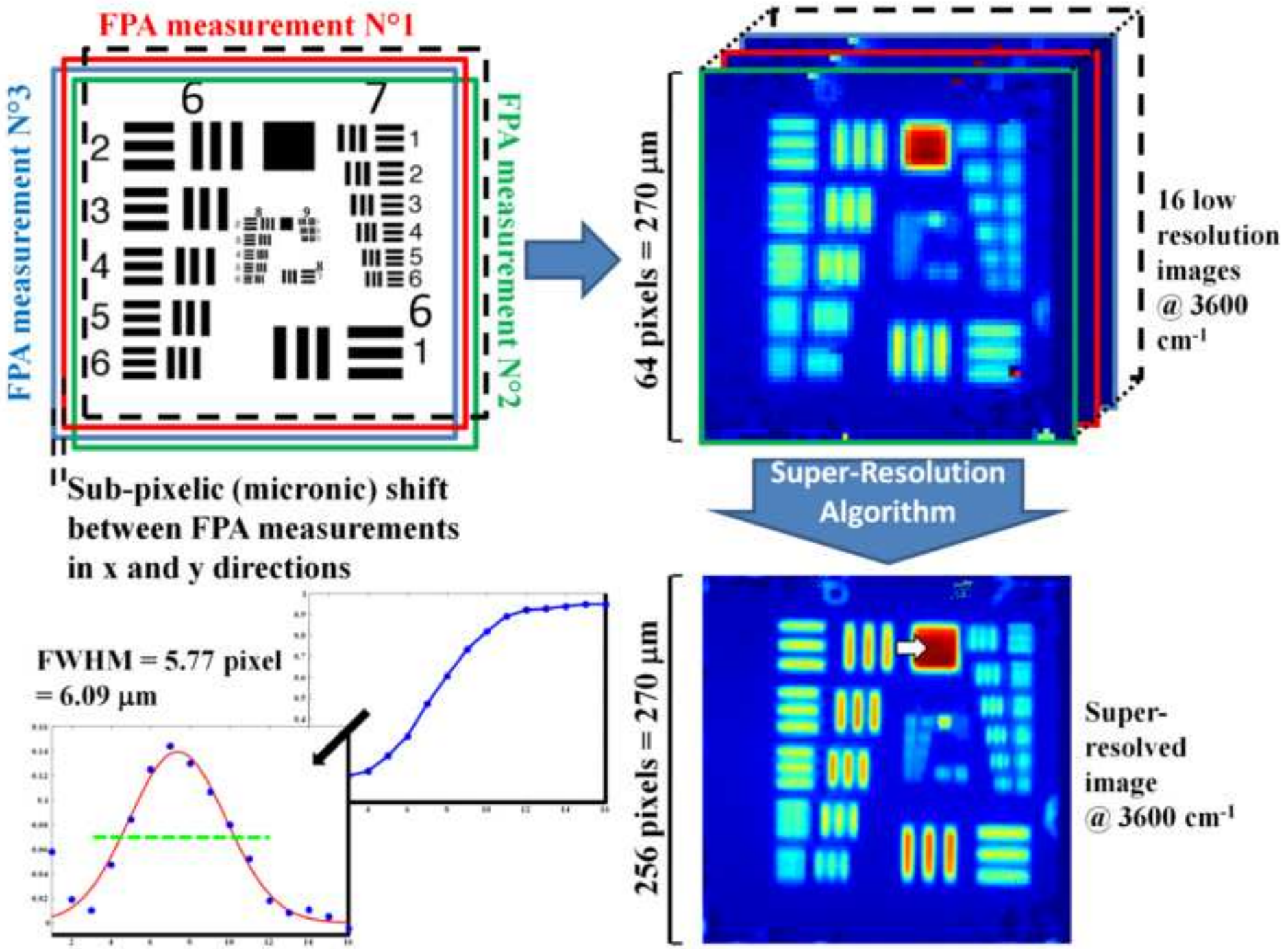
FPA measurement N°1
FPA measurement N°2
FPA measurement N°3
Sub-pixelic (micronic) shift between FPA measurements in x and y directions
64 pixels = 270 µm
16 low resolution images @ 3600 cm-1
Super-Resolution Algorithm
256 pixels = 270 µm
Super-resolved image @ 3600 cm-1
FWHM = 5.77 pixel = 6.09 µm

Figure 6

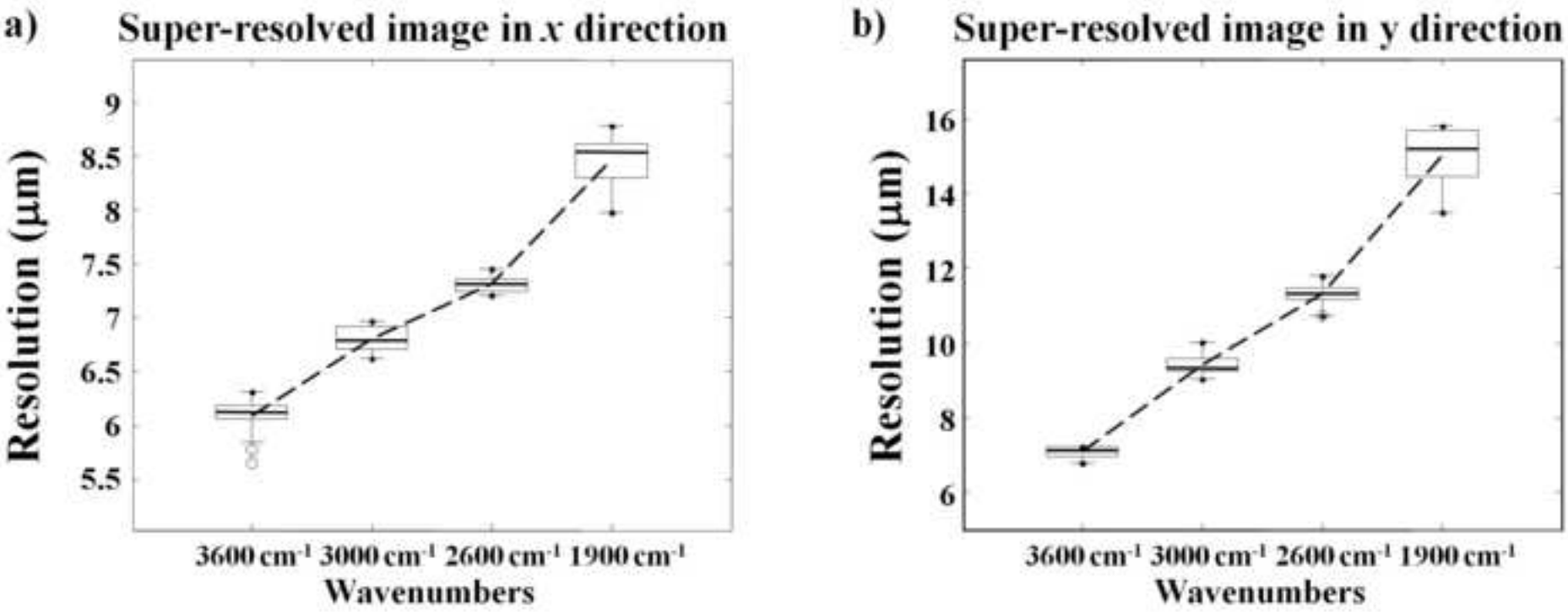
a)
Super-resolved image in x direction
Resolution (μm)
9
8.5
8
7.5
7
6.5
6
5.5
3600 cm-1 3000 cm-1 2600 cm-1 1900 cm-1
Wavenumbers
b)
Super-resolved image in y direction
Resolution (μm)
16
14
12
10
8
6
3600 cm-1 3000 cm-1 2600 cm-1 1900 cm-1
Wavenumbers

Figure 7

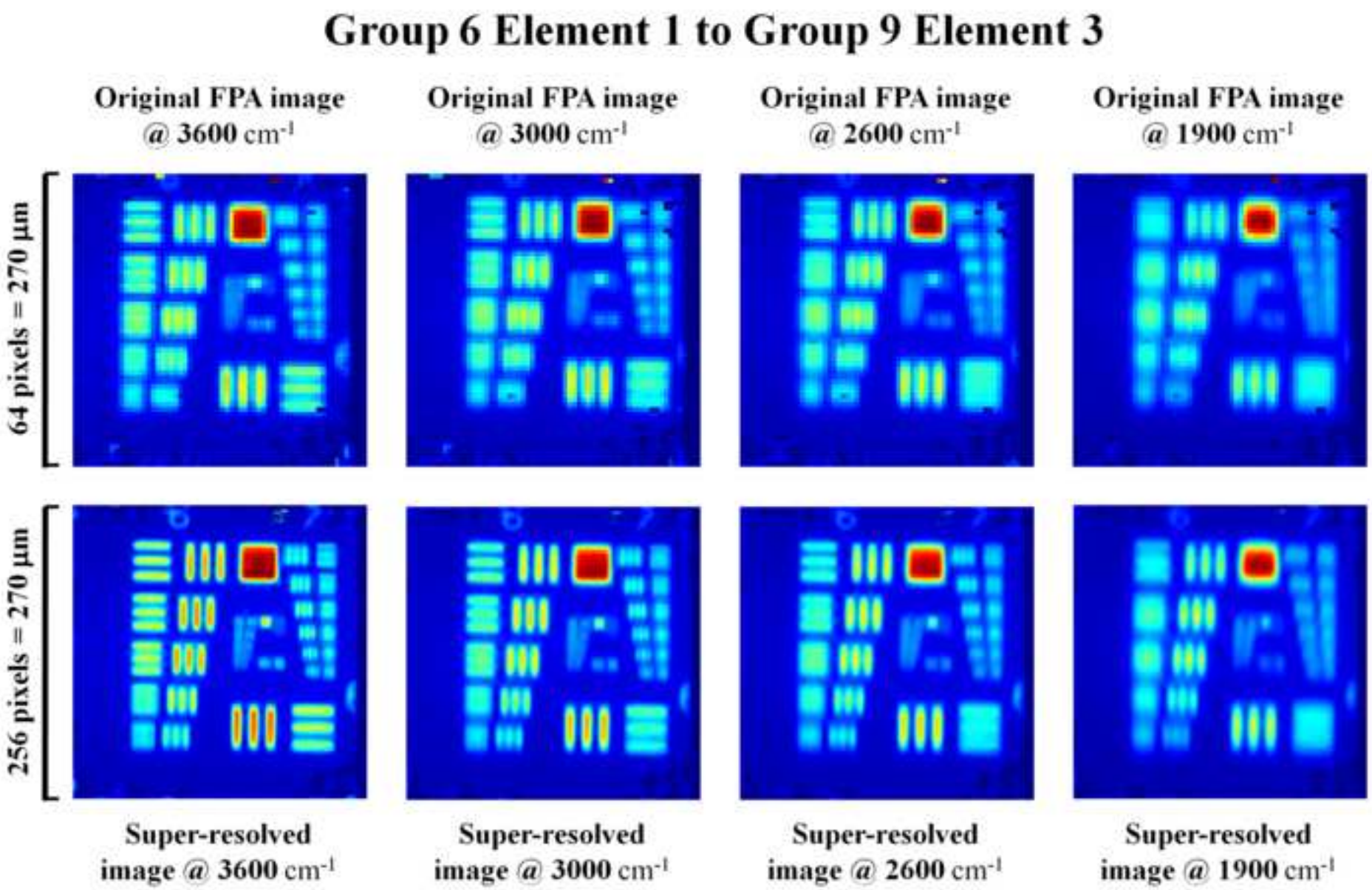
Group 6 Element 1 to Group 9 Element 3
Original FPA image @ 3600 cm-1
Original FPA image @ 3000 cm-1
Original FPA image @ 2600 cm-1
Original FPA image @ 1900 cm-1
64 pixels = 270 µm
256 pixels = 270 µm
Super-resolved image @ 3600 cm-1
Super-resolved image @ 3000 cm-1
Super-resolved image @ 2600 cm-1
Super-resolved image @ 1900 cm-1